
JOINT INVERSION OF CRUSTAL AND UPPERMOST MANTLE STRUCTURE IN WESTERN CHINA

Xiaodong Song, et al.

**University of Illinois
Department of Geology
605 E. Springfield Ave.
Champaign, IL 61820**

2 November 2013

Final Report

APPROVED FOR PUBLIC RELEASE; DISTRIBUTION IS UNLIMITED.



**AIR FORCE RESEARCH LABORATORY
Space Vehicles Directorate
3550 Aberdeen Ave SE
AIR FORCE MATERIEL COMMAND
KIRTLAND AIR FORCE BASE, NM 87117-5776**

DTIC COPY

NOTICE AND SIGNATURE PAGE

Using Government drawings, specifications, or other data included in this document for any purpose other than Government procurement does not in any way obligate the U.S. Government. The fact that the Government formulated or supplied the drawings, specifications, or other data does not license the holder or any other person or corporation; or convey any rights or permission to manufacture, use, or sell any patented invention that may relate to them.

This report was cleared for public release by the 377 ABW Public Affairs Office and is available to the general public, including foreign nationals. Copies may be obtained from the Defense Technical Information Center (DTIC) (<http://www.dtic.mil>).

AFRL-RV-PS-TR-2014-0024 HAS BEEN REVIEWED AND IS APPROVED FOR PUBLICATION IN ACCORDANCE WITH ASSIGNED DISTRIBUTION STATEMENT.

//SIGNED//

Robert Raistrick
Project Manager, AFRL/RVBYE

//SIGNED//

Edward J. Masterson, Colonel, USAF
Chief, Battlespace Environment Division

This report is published in the interest of scientific and technical information exchange, and its publication does not constitute the Government's approval or disapproval of its ideas or findings.

REPORT DOCUMENTATION PAGE

Form Approved
OMB No. 0704-0188

Public reporting burden for this collection of information is estimated to average 1 hour per response, including the time for reviewing instructions, searching existing data sources, gathering and maintaining the data needed, and completing and reviewing this collection of information. Send comments regarding this burden estimate or any other aspect of this collection of information, including suggestions for reducing this burden to Department of Defense, Washington Headquarters Services, Directorate for Information Operations and Reports (0704-0188), 1215 Jefferson Davis Highway, Suite 1204, Arlington, VA 22202-4302. Respondents should be aware that notwithstanding any other provision of law, no person shall be subject to any penalty for failing to comply with a collection of information if it does not display a currently valid OMB control number. **PLEASE DO NOT RETURN YOUR FORM TO THE ABOVE ADDRESS.**

1. REPORT DATE (DD-MM-YYYY) 02-11-2013			2. REPORT TYPE Final Report		3. DATES COVERED (From - To) 30 Mar 2010 to 30 Sep 2013	
4. TITLE AND SUBTITLE Joint Inversion of Crustal and Uppermost Mantle Structure in Western China					5a. CONTRACT NUMBER FA9453-10-C-0216	
					5b. GRANT NUMBER	
					5c. PROGRAM ELEMENT NUMBER 62601F	
6. AUTHOR(S) Xiaodong Song, Jiangtao Li, Zhen J. Xu, Lupei Zhu*, Yumei Zhou*					5d. PROJECT NUMBER 1010	
					5e. TASK NUMBER PPM00000936	
					5f. WORK UNIT NUMBER EF002221	
7. PERFORMING ORGANIZATION NAME(S) AND ADDRESS(ES) University of Illinois Department of Geology 605 E. Springfield Ave. Champaign, IL 61820					8. PERFORMING ORGANIZATION REPORT NUMBER *Saint Louis University 221 N. Grand Boulevard St. Louis, MO 63103	
9. SPONSORING / MONITORING AGENCY NAME(S) AND ADDRESS(ES) Air Force Research Laboratory Space Vehicles Directorate 3550 Aberdeen Ave. SE Kirtland AFB, NM 87117-5776					10. SPONSOR/MONITOR'S ACRONYM(S) AFRL/RVBYE	
					11. SPONSOR/MONITOR'S REPORT NUMBER(S) AFRL-RV-PS-TR-2014-0024	
12. DISTRIBUTION / AVAILABILITY STATEMENT Approved for public release; distribution is unlimited. (377ABW-2014-0205 dtd 31 Mar 2014)						
13. SUPPLEMENTARY NOTES						
14. ABSTRACT This research is to develop joint-inversion methods involving P travel times, receiver functions, and surface wave dispersion measurements and to apply them to the western China region to obtain 3D models of P and S structures of the crust and upper mantle. We successfully implemented a search-based algorithm (neighborhood algorithm) for joint inversion of surface wave dispersion data, receiver functions, and Pn delay time. The implementation uses parallel programming with MPI calls, making massive data processing possible. We have systematically carried out individual components of the project, obtaining unprecedented data sets for surface wave dispersion, receiver functions, and Pn tomography, needed for the joint inversion. We have tested the joint inversion method and proposed a practical strategy for the joint inversions of the real data. We obtained detailed joint inversion results for the dense HiClimb array, which are generally consistent with previous results but show considerable difference in details (crustal structure and Moho depths). We have performed systematically joint inversions of all available stations in western China and obtained 3D S velocity model, average crustal Vp/Vs map, and derived 3D P velocity model of the region.						
15. SUBJECT TERMS joint inversion, surface waves, receiver functions, Pn tomography						
16. SECURITY CLASSIFICATION OF:			17. LIMITATION OF ABSTRACT	18. NUMBER OF PAGES	19a. NAME OF RESPONSIBLE PERSON Robert Raistrick	
a. REPORT Unclassified	b. ABSTRACT Unclassified	c. THIS PAGE Unclassified			19b. TELEPHONE NUMBER (include area code)	
			Unlimited	30		

This page is intentionally left blank.

Table of Contents

1. Summary	1
2. Introduction.....	1
3. Technical Approach.....	2
3.1 Sensitivity tests	2
3.2 Implementation of the joint inversion method.....	2
3.3 Data preparation.....	3
3.4 Practical considerations for an implementation for real data.....	3
3.5 Computation considerations.....	6
4. Results and Discussion	6
4.1 Dispersion measurements, dispersion maps, and 3D S model.....	6
4.2 Receiver functions	7
4.3 Pn Tomography.....	7
4.4 Joint Inversions	9
5. Conclusions.....	11
References.....	22

List of Figures

Fig. 1. An example of commonly-used joint inversion of receiver functions and surface wave dispersion.....	12
Fig. 2. Synthetic tests on combining Pn station delays with receiver functions and surface wave dispersion for a joint inversion	12
Fig. 3. Synthetic test of joint inversion including receiver functions, surface wave dispersion and Pn delay time data using the Neighborhood Algorithm.....	13
Fig. 4. Distributions of seismic stations (triangles) and earthquakes (stars) used for joint ambient noise and earthquake surface wave tomography	13
Fig. 5. Group velocity maps at 10, 30, and 50 s using EGFs and earthquake data (left) and earthquake data only (right)..	14
Fig. 6. S velocity maps at different depths from our inverted model.	15
Fig. 7. S velocity cross-sections of our model in western China.....	16
Fig. 8. Stations for which receiver functions have been systematically processed and obtained for the joint inversion of this project.....	17
Fig. 9. Results of preliminary Pn tomography in western China.....	17
Fig. 10. Crustal thickness along the profile of HI-CLIMB stations.....	18
Fig. 11. Test result of joint inversion with Pn data on HiClimb station H1620.....	18
Fig. 12. Tests of Pn weighting on the inversion results (using HiClimb station H1620).	19
Fig. 13. Tests of model sensitivities to Vp/Vs ratio and with/without Pn data constraint.	19
Fig. 14. Vp/Vs ratios derived from joint inversion of surface wave dispersion, receiver functions, and Pn station delays	20
Fig. 15. Results of joint inversion for the Hi-CLIMB array (A, B).....	20
Fig. 16. Map of Vp/Vs ratios in western China obtained in this study.....	21
Fig. 17. Maps of the P velocity model of western China from this project.	21

1. Summary

The objective of this research is to develop joint-inversion methods involving P travel times, receiver functions, and surface wave dispersion measurements and to apply them to the western China region to obtain 3D models of P and S structures of the crust and upper mantle. Our joint inversion methods involve obtaining Pn station delays, which are then used with surface wave dispersion and receiver functions at each station to invert jointly for S structure, the Moho depth, and Vp/Vs ratios in the crust. Our main accomplishments include the following four areas. (1) We successfully implemented a search-based algorithm (neighborhood algorithm) for joint inversion of surface wave dispersion data, receiver function, and Pn delay time. The implementation uses parallel programming with MPI calls, making massive data processing possible. (2) We have systematically carried out individual components of the project, obtaining unprecedented data sets for surface wave dispersion, receiver functions, and Pn tomography, needed for the joint inversion. (3) We have tested the joint inversion method and proposed a practical strategy for the joint inversions of the real data. We obtained detailed joint inversion results for the dense HiClimb array, which are generally consistent with previous results but show considerable difference in details (crustal structure and Moho depths). (4) We have performed systematically joint inversions of all available stations in western China and obtained a 3D S velocity model, an average crustal Vp/Vs map, and derived a 3D P velocity model of the region.

2. Introduction

The objective of this research is to develop joint-inversion methods involving P travel times, receiver functions, and surface-wave dispersion measurements from ambient noise correlation and to apply them to the western China region to obtain 3D models of P and S structures of the crust and upper mantle.

In seismic inversion, trade-offs between model parameters are well known. To resolve the ambiguity and to improve resolution, a combination of different data sets that have sensitivities to different parameters is required or a priori constraints have to be imposed. For example, it has long been recognized that teleseismic P receiver functions are primarily sensitive to shear-wave velocity (Vs) contrasts and the depth-velocity product, and not the velocity alone (Ammon et al., 1990). On the other hand, surface waves are primarily sensitive to the vertical shear-velocity averages. Thus, joint inversion (or analysis) of receiver functions and surface wave dispersion has now been commonly used to resolve depth resolution of Vs structure (e.g., Julia et al. 2000; Ozalaybey et al., 1997). Similarly, crustal thickness estimated using only the delay time of the Moho P-to-S converted phase (Ps) relative to P at the receiver trades off strongly with the crustal Vp/Vs ratio, which can be remedied using later converted phases (Zhu and Kanamori, 2000).

In this project, we obtain and exploit a vast collection of data that we have access to for western China and have accumulated over decades. The data includes P travel times, P receiver functions, Rayleigh wave group and phase velocities from both earthquakes and ambient noise. We then combine individual data components into a joint inversion to derive P and S crustal models. In particular, we add additional P information (Pn delay times) in the joint inversion of receiver functions and surface wave dispersion to obtain an S model profile and average crustal Vp/Vs ratios for stations that have the three types of data. Essentially, the inclusion of the station delay from the Pn inversion provides an additional constraint on the Moho depth and average crustal P velocity in the joint inversion with receiver functions and surface wave dispersions.

3. Technical Approach

We have implemented a joint inversion method that includes surface wave dispersion data, receiver functions, and Pn station delay time. A feature of this joint inversion is that all the individual components (surface wave dispersion, receiver function, and Pn delay time) are quantified with respect to the same station of interest. Below we describe in detail the joint inversion method (see also Xu et al., 2013a).

3.1 Sensitivity tests

The combination of receiver functions and surface wave dispersion bridges some resolution gaps associated with each individual data set (e.g., Julia et al. 2000; Ozalaybey et al., 1997). **Fig. 1** shows an example of joint inversion of receiver functions and surface wave dispersion at an INDEPTH station. However, important ambiguity remains. In the P receiver function, the Moho P-to-S converted phase (Ps) is generally the strongest. The Moho depth determined from the Ps delay (relative to P) trades off strongly with the crustal Vp/Vs ratio. Multiple converted phases would help resolving the ambiguity (Zhu and Kanamori, 2000), but they are usually more difficult to identify. Sensitivity tests (**Fig. 2**) suggest that adding well-constrained P information will help the joint inversion of receiver function and surface wave dispersion to find the right S model when the Vp/Vs ratio is not known, which is often the case. One type of P information is the Pn station delay time, which provides constraint on Moho depth and average crustal velocity. This is the type of P information we focus on in this project.

3.2 Implementation of the joint inversion method

We have successfully implemented a joint inversion method that includes surface wave dispersion data, receiver functions, and Pn delay times that are associated with the same station of interest. The implementation includes the following key elements. (1) We use fast global search method, the neighborhood algorithm (NA) (Sambridge, 1999). Using a global parameter search approach, compared with a more traditional linearized iterative inversion approach, has two key advantages: (a) We have more control on parameterization, for example, to include Pn data, we need to define a Moho; and (b) we are able to explore parameter space more fully and to quantify the resolution and

uncertainty of the solution more easily. (2) Our parameterization includes the Moho, the depth of which is allowed to vary. It can include variable crustal layers as well. Regions between layers are parameterized as smooth functions (linear or splines) to reduce the number of search parameters. (3) The implementation uses parallel programming with MPI calls, which greatly speeds up the model search with multi-processor or parallel machines. **Fig. 3** shows a synthetic example using the global search method for joint inversion of surface wave and receiver functions and Pn delay time. The method finds a solution with perfect fit to the input model and data.

3.3 Data preparation

We use the HiClimb data to test our joint inversion implementation. This is a large volume of data (some 180 stations), and we need an effective procedure to obtain each data set for the joint inversion. **First**, we obtained high resolution dispersion curves along the array using a linear array inversion procedure. Because, it's a near-linear dense array, we can reduce the 3D structure inversion problem to a 2D problem along the array, thus allowing us to refine the grid size (to 0.1 degree). We implemented a version of ambient noise surface wave tomography that is suitable for a dense linear array. **Second**, we constructed receiver functions for all the stations using the semi-automatic procedure described in section 4.2. The interactive procedure allowed us to control data quality but also to increase efficiency, which is essential to processing a large volume of data. For each receiver function, we also extract the delay time of the Moho-converted phase Ps relative to the reference phase P from the H-K stacking procedure (Zhu and Kanamori, 2000). Although the crustal thickness from the receiver function trades off strongly with the Vp/Vs ratio, the Ps delay time is robust as long as the converted phase is strong enough. The delay time provides an efficient constraint on the model search by ruling out models with significant differences in the delay time. **Third**, our joint inversion method includes Pn station delay times obtained from Pn tomography of the whole of western China (see below).

3.4 Practical considerations for an implementation for real data

Below we describe practical considerations in the implementation for real data (with HiClimb data as an example). Particular effort was made in formulating effective procedures and in model parameterization. Although a search-based approach provides great flexibility in fitting different types of data, it is generally very expensive computationally. The selection of parameterization requires particular care because of the need to limit the number of parameters.

Derivation of starting model. Our joint inversion is done in two steps. In the first step, we invert only the dispersion data to obtain a starting S velocity profile at each station, which is then used as the starting model for the model searches. The main purpose of the starting model is to reduce the model space to help the search algorithm converge faster. We use cubic splines for model parameterization. The advantage of using splines is that they yield a naturally smooth model and yet reduce the number of parameters for searching.

For the dispersion inversion in the first step, we adopt 12 uniformly distributed spline nodes from the surface down to 150 km. We seek the solution that satisfies the following minimizer:

$$\min (\|\mathbf{D}^{\text{obs}} - \mathbf{D}^{\text{pred}}\| + \lambda \|\mathbf{m}\| + \varphi \|\mathbf{Lm}\|) \quad (1),$$

where the first term is data misfit, \mathbf{D}^{obs} is the data (dispersion curve) we are trying to fit, and \mathbf{D}^{pred} is the predictions from the random model generated by the NA algorithm. The second term is the model constraint. Since the dispersion periods of the HiClimb data from the ambient noise extends only up to 45 s, which has limited constraint on the deeper part of the structure, we introduce a model constraint for the depth from 95 km down to 150 km using an S model of China and the surrounding region, which includes group velocity period up to 120 s (Xu et al., 2013b). The third term is the smoothing constraint. \mathbf{L} is the Laplacian smoothing operator (Lees and Crosson, 1989), which requires the second derivative of the model to be zero. λ and φ are two real positive numbers that have been chosen so that different terms are well balanced. We seek the solution that minimizes the L1 norm of above formula instead of the traditional L2 norm. The choice of the L1 norm reduces the risk that the model is biased by extreme values due to error in the data. We convert the spline model into a layered velocity model to calculate predicted Rayleigh group and phase velocities. We divide the whole 150 km into 30 layers with 5 km thickness for each layer. Velocity within each layer is constant. We fix the V_p/V_s ratio for all the layers to 1.75. Density is calculated by the Nafe-Drake (1963) relationship. The forward calculation subroutine is adopted from Robert Herrmann's program (1991).

Joint inversion. The parameterization for the second step in the joint inversion is different from the first step. We use two sets of cubic splines to represent the velocity model: one for the crust (first set) and one for the Moho and the mantle (second set). The last node of the first spline has the same value as the first node of the second spline so that the model is continuous throughout the depth. The node spacing for each set of spline is not uniform; instead, it is stretched over depth, with closer spacing between nodes at the top of the spline and larger spacing at the bottom of the spline. We use the following formula to map the normalized spline space (0 to 1) to the depth:

$$h = Dx^2 + h_0 \quad (2),$$

where h is the depth from the top of the first node in the spline; D is the total thickness; h_0 is the depth of the first node; x is the coordinate in the normalized spline space between 0 and 1. This set up is effective in modeling the structure at shallow depth and near the Moho discontinuity region by giving more freedom to the model where it is better constrained by short period dispersion data and receiver functions, respectively. It also yields a smoother model at the lower crust and deeper mantle, which are less constraint by the data. We use 12 nodes for the first spline in the crust and 10 nodes for the second spline in the Moho and the mantle. We also allow the depth of the connecting node between the first and the second splines to vary so that the Moho depth can be adjusted.

The use of the Moho and mantle spline provides more flexibility compared with a Moho with an imposed discontinuity or linear gradient. For a Moho depth at 70 km, the node spacing between the first and second nodes in the mantle is ~ 0.99 km and the spacing between the second and third nodes is ~ 2.96 km, enough to model a sharp velocity jump, thus mimicking the Moho discontinuity. On the other hand, this parameterization also works well in the situation where the Moho is not sharp but presents as a transition zone. We convert the spline model into layered model as in the first step. We use 2 km layer thicknesses throughout the depth range of the first spline in the crust. In the mantle, we use fifteen 2 km layers for the top 30 km as a transition zone followed by 5 km layers to the bottom at 150 km. We seek the solution that satisfies the L1 norm of the following minimizer:

$$\min(w_1 \|\mathbf{D}_{\text{disp}}^{\text{obs}} - \mathbf{D}_{\text{disp}}^{\text{pred}}\| + w_2 \|\mathbf{D}_{\text{rfs}}^{\text{obs}} - \mathbf{D}_{\text{rfs}}^{\text{pred}}\| + w_3 \|\mathbf{D}_{\text{delay}}^{\text{obs}} - \mathbf{D}_{\text{delay}}^{\text{pred}}\| + \lambda \|\mathbf{m} - \mathbf{m}_0\| + \varphi \|\mathbf{Lm}\|) \quad (3),$$

where the first term is the dispersion misfit, the second term is the RFs misfit and the third and last terms are the same as formula (1). The w_1 , w_2 and w_3 are the relative weighting for dispersion, RFs and Pn delay time misfits, respectively.

We impose model-screening algorithms to speed up model convergence. Every time NA generates a random model, we compare the model with the starting model from the dispersion inversion for each layer except those 15 layers in the transition zone. If the velocity difference in any given layer is larger than 0.5 km/s, this model is discarded by setting a large misfit value without going through the forward calculation. We also require the velocity to increase monotonically from the last two nodes in the crust to first two nodes in the mantle. This model screening process can reduce computational time by confining the model search in the model space where the likelihood of the model is the largest.

Another screening parameter is the measured Ps delay time. Because the converted Ps phase may be mis-identified in the H-K stacking process, we need to sort out the “outliers” of the Ps delay times before applying the screening. We fit the measured Ps delay times of all the stations with a smooth spline curve. If the measurement for a station is different from the prediction of the spline fit by more than 1.5 s, then we use the spline prediction as the Ps delay time for that station, otherwise we use the original Ps delay measurement. For each model generated in the search, we calculate the velocity gradient from each layer to the next layer and pick the one with largest gradient as the “Moho”. In most cases, it is the last layer in the first spline to the first layer in the mantle spline. We calculate the predicted Ps delay time using the “Moho” defined above and compare it with the measured Ps delay. If the difference is larger than 1 s, then the model is discarded (assigned a large misfit value). Our experience suggests that by introducing the Ps delay time, the model converges faster than without the Ps delay screening.

The density of each layer is calculated using the same Nafe-Drake relationship as described above. Because of the lack of coherent crust multiple signals, only the first 15 s of receiver functions are included in inversion. For each station, we select 4 receiver

functions with different ray parameters for inversion. The move out of Ps signal at different ray parameters is helpful in determining the Moho depth. Subroutines of dispersion and receiver function forward calculation are adopted from Robert Herrmann's computer programs. We iterate 800 times to obtain the final model and 100 new models are generated each iteration in 5 Voronoi cells.

3.5 Computation considerations

The project involves a tremendous amount of data and computation, so special considerations on computational efficiency and computational resources are needed. First, we spent considerable effort in speeding up the calculations of empirical Green functions of surface waves from noise correlations. Because the task for each pair is quite independent, it can be parallelized efficiently. The main obstacle is lots of I/O operations, which require expensive reading and writing hard drives. We have come up a solution that would speed up the computation by distributing tasks to multi-processors within the same computer (node) and execute them simultaneously. The method uses the LINUX POSIX message queue (mq) capabilities. Second, we developed a semi-automatic procedure to generate receiver functions. Because of large number of stations and large amount of data, such a procedure is essential for productivity (see below). Third, the joint inversion is based on MPI-calls, which can be run on parallel machines. We used a Linux cluster in our institution and the National Center for Supercomputing Applications on the University of Rhode Island campus for most of the computations.

4. Results and Discussion

We now summarize briefly the results of the individual components of surface wave dispersion, receiver functions, and Pn tomography and describe in some detail the joint inversion results.

4.1 Dispersion measurements, dispersion maps, and 3D S model

We have systematically measured dispersion for the construction of dispersion maps from ambient noise correlations as well as traditional earthquake data. The stations include the Chinese national backbone stations and open permanent and temporary stations from the early 1990s with a total of over 500 stations (**Fig. 4**). Earthquake data include events greater than magnitude 5.0 from 2000 to 2007. The total dataset has dispersion measurements for the period from 8 s to 120 s with a maximum of ~35000 measurements for group velocity and ~22500 measurements for phase velocity at the period of 20 s.

Dispersion maps at different periods are constructed by minimizing the following equation:

$$\min (||\mathbf{A}\mathbf{m}-\mathbf{r}||^2+\lambda^2||\mathbf{m}||^2+\varphi^2||\mathbf{L}\mathbf{m}||^2)$$

The first term is data misfit, in which \mathbf{m} is the parameter vector, \mathbf{A} is the coefficient matrix, \mathbf{r} is the vector of travel time residuals. The second term is the model regularization with a damping parameter of the non-zero real number λ . The third term is the smoothing constraint with the non-zero real number φ . The smoothing operator \mathbf{L} is the Laplacian operator (Lees and Crosson, 1989).

Examples of new dispersion maps are shown in **Fig. 5**. Earthquake data account for about 50% of the total group velocity measurements for periods from 8 to 70 s. We compare group velocity dispersion maps from earthquake data and the results using the whole data set. All large-scale major features are similar, e.g. low velocity in sedimentary basins at short periods, a low velocity zone throughout the Tibetan Plateau, and an east-west velocity contrast at mid periods, although there are differences in detailed structures.

We invert the dispersion maps for a 3D S velocity model. Figs. 6-7 show some S velocity maps and profiles, respectively. A detailed discussion of the main features of the model can be found in Xu et al. (2013b).

4.2 Receiver Functions

We have systematically processed receiver functions of stations in Western China (Fig. 8), using a semi-automatic procedure we have developed to generate receiver functions. The procedure includes interactive review and selection of good quality raw data using a graphic interface, picking and alignment of P waveforms using waveform cross-correlation and a graphic interface, automatic calculations of receiver functions and stackings according to ray parameters and azimuths, and interactive selections of good quality receiver functions using a graphic interface.

4.3 Pn Tomography

We have worked systematically on Pn waves. Our data come from three sources: 1) Chinese bulletin data, 2) international bulletin data (ISC), and 3) hand-picked data at temporary and permanent stations. Distribution of permanent stations in western China (even including regional and provincial networks in China) is quite sparse. However, there have been a number of PASSCAL experiments in Western China. These stations

are usually in remote areas where permanent stations are lacking, providing complimentary ray coverage.

For hand-picking, we designed an inter-active scheme to pick Pn arrival times semi-automatically. It involves inspecting original seismograms (vertical component, filtered at 0.2 to 3 Hz), discarding noisy traces, zooming in Pn arrivals, picking each trace by hand, plotting travel-time curves and reduced travel-time curves, and double-checking picks if there are obvious anomalies. We have examined about 200 shallow events (depth less than 40 km) with magnitude greater than 5.5 over 15 years (1995-2009) in the region from 25 to 56 deg north and 68 to 108 deg east. We require epicentral distances to be from 2 to 12 degrees and at least 10 Pn picks for each event. We picked over 1800 Pn arrivals from 81 events.

We combine the three data sources and impose the following data selection criteria for the combined data set. (1) Earthquakes whose depth is over 45 km are discarded. (2) The apparent velocity of rays is limited between 7.0 and 9.0 km/s. (3) To ensure robust constraint on the station delays, we keep the stations with at least 5 Pn picks and keep the earthquakes with at least 5 Pn records. (4) We use an earthquake-grouping technique (Liang et al., 2004) to locate earthquake clusters, then choose the earthquake with the largest number of Pn picks in a cluster and exclude all the other earthquakes in the same cluster. After the data selection, we obtain 54,849 rays from 398 stations and 6,220 earthquakes.

For Pn tomography, we follow the basic approach of parameterizing the Pn residual into mantle perturbation, the earthquake term, and the station term (e.g., Hearn, 1996; Liang et al., 2004; Liang and Song, 2006). For the initial model of inversion, we choose average crustal velocity of 6.3 km/s, average Pn velocity of 8.06 km/s, and average Moho depth of 51 km (Liang and Song, 2006). We divide the study region into $1^\circ \times 1^\circ$ 2-D grids.

The inversion results of Pn velocities and station delays are shown in Fig. 9. The Pn velocity map (Fig. 9A) shows a number of significant features consistent with the geology of the region and previous studies, including high Pn velocity anomalies in four major basins (Sichuan, Tarim, Qaidam, and Junggar basin), high uppermost mantle velocities in the southern Tibetan Plateau (TP), low Pn velocities in northern TP, and a striking low velocity belt extending from west to east beneath northern TP to the eastern and southeastern margins of the plateau, observed previously by Liang and Song (2006). The station delays vary greatly in the study region (Fig. 9B), suggesting large changes in crust thickness, as we expect.

The station delays provide a critical data set for our joint inversion with surface waves and receiver functions. We can examine the constraint of the Pn station delay time by examining the crustal thickness estimated using the station delay alone.

The station delay is related to the crustal velocity (v_c), crustal thickness (H), and the reference model (\bar{v}_c , \bar{H}) as follows: $t_\eta - \bar{t}_\eta = H \sqrt{\frac{1}{v_c^2} - \frac{1}{v_m^2}} - \bar{H} \sqrt{\frac{1}{\bar{v}_c^2} - \frac{1}{v_m^2}}$

where $\eta = \left(\frac{1}{v_c^2} - \frac{1}{v_m^2} \right)^{1/2}$, is the vertical slowness in the crust. If we assume an average crustal velocity, we can estimate the crustal thickness. **Fig.10** shows a comparison of the crustal thickness along HiClimb stations estimated from three data sets: Pn station delay, receiver function, and joint inversion of surface wave dispersion and receiver function. We see that the crustal thickness derived from different data sets is mutually consistent in general. There are, however, some discrepancies, which likely arise from the uncertainties in the crustal velocities and which we hope to resolve with joint inversions of all the data sets.

4.4 Joint Inversions

Combining individual components described above, we now focus on joint inversions of surface wave dispersion, receiver function, and Pn delay time.

1) Tests on joint inversions.

We first conduct various tests of the joint inversions. Key considerations include: (1) the inclusion of the Vp/Vs ratio in the search parameter in the coding, (2) the relative weighting between different types of data (dispersion, receiver function, and Pn delay time), (3) the difference of model results with or without the Pn data, (4) the robustness of the joint inversion.

Fig. 11 shows an example of the joint inversion for a HiClimb station. The joint inversion with Pn shows a very similar S velocity profile to that of the joint inversion with surface wave dispersion and receiver function only. The predictions fit to the observed dispersion data and to receiver functions very well. The fits are not distinguishable from the results of the joint inversion using the dispersions and receiver functions only. However, we note that there is a noticeable difference in Moho depth due to a difference in the best-fit Vp/Vs ratio (1.83 compared to a assumed value of 1.75 in the dispersion and receiver function inversion). The example underlines the importance of including P constraints in the joint inversion.

A certain question to ask is how robust the derived Vp/Vs ratio from the joint inversion is. We thus conduct another test with different weightings on the Pn data in the total misfit function (**Fig. 12**). Our tests show that the derived Vp/Vs ratio is quite robust for a range of Pn data weightings when the quality of receiver functions is good. However, the

sharpness of the Moho varies. Essentially, the V_p/V_s ratio is constrained by the timing of dispersion, the P_s delay times in the receiver functions, and the P_n delay time. However, the sharpness of the Moho affects the amplitudes of the P_s in the receiver functions. A greater P_n weighting down-weights the receiver function in the misfit, thus the receiver functions are not fit as well.

Yet another test is the effect of the V_p/V_s ratio and the inclusion and exclusion of P_n data on the model inversion, shown in **Fig. 13** for a HiClimb station H1350. In previous inversion with the availability of the P_n delay time, we set the initial V_p/V_s value to be 1.75 and the inversion result from surface wave and receiver functions is shown in blue. With the addition of the P_n delay time, we found the optimal V_p/V_s value of 1.88. As a result, the inversions (red and green) with the optimal V_p/V_s of 1.88 yield significantly different Moho depth and uppermost mantle structures than the initial inversion. However, the inclusion of P_n delay time also down-weights the dispersion and receiver function data in the total misfit function. As a result, the joint inversion with the P_n data included yields a more gradual Moho (green) and smaller P_s amplitude in the receiver function (**Fig. 13**). However, if we use the new V_p/V_s ratio of 1.88 and include only the dispersion and receiver function data, we obtain a similar S velocity profile as in the joint inversion as well as a sharper Moho, which fits the receiver function P_s amplitude better.

2) Strategies for the joint inversions

From the above tests, we outline our strategies for the joint inversion of real data. For a “good” station that has all the three types of data (surface wave, receiver function, and P_n delay time) and the Moho conversion is strong in the receiver functions, we first use all the data to derive an optimal V_p/V_s ratio, and then fix the V_p/V_s ratio at the optimal value and conduct a separate inversion using dispersions and receiver functions only. For other stations, we use our best estimates of the V_p/V_s ratios based on the “good” stations and perform the joint inversions of dispersions and receiver functions only.

3) Joint inversion results: HiClimb stations

Fig. 14 shows V_p/V_s ratios derived from HiClimb stations. The results that use all the stations that have the three types of data (about 60 stations) (open circles) are consistent with those from a subset of stations that have the “best” receiver functions (with strong Moho conversions) (solid dots). The derived V_p/V_s ratios show large variations from the collision front across the Tibetan Plateau (TP). The V_p/V_s ratios in the TP is significantly greater than in the Indian Shield. However, the ratios in the Lhasa Block are significantly smaller than in the Himalaya and Qiangtang Blocks.

Fig. 15 shows results of the joint inversion of the three types of data for HiClimb stations. The joint inversion (**Fig. 15A**) is generally consistent with the joint inversion of dispersions and receiver functions only (**Fig. 15B**) or the inversion of the dispersions

only (Fig. 15C). But there are some noticeable differences in mid-crustal low velocity zone structure and in Moho depth.

4) Joint inversion results: western China

Using the strategy outlined above, we have systematically performed joint inversions for each station that has all the three types of data (surface wave, receiver function, and Pn delay time). From the joint inversion, we obtain an optimal Vp/Vs ratio for each station. These Vp/Vs ratios are then interpolated to derive a Vp/Vs map (**Fig. 16**). Note because of non-uniform distribution of stations for which we can perform the joint inversions, the derived Vp/Vs ratio map is highly uncertain. However, we do observe consistent large-scale patterns. In particular, the Vp/Vs ratios are anomalously high for western TP compared to surrounding regions.

An important limitation of the joint inversion method is that it's limited by station distributions. However, because of excellent coverage of surface wave dispersions for the 3D S velocity model and our derived Vp/Vs map, we can derive a 3D P velocity model (**Fig. 17**) based on the 3D S velocity model and the Vp/Vs map. The derived 3D P model shows distinct geological features of tectonic blocks, which mimics features from the 3D S model with some modifications. In the future, it would be useful to compare and integrate such a derived P model with P travel-time derived models for the region.

5. Conclusions

We successfully developed and implemented a search-based algorithm (NA) for joint inversion of surface wave dispersion data, receiver functions, and Pn delay times using parallel programming. We obtained unprecedented data sets for surface wave dispersion, receiver functions, and Pn tomography, needed for the joint inversion. We tested the joint inversion method and proposed a practical strategy for joint inversions of the real data. We obtained detailed joint inversion results for the dense HiClimb array, which are generally consistent with previous results but show considerable difference in details (crustal structure and Moho depths). We have systematically performed joint inversions of all available stations in western China and obtained a 3D S velocity model, an average crustal Vp/Vs map, and a derived 3D P velocity model of the region.

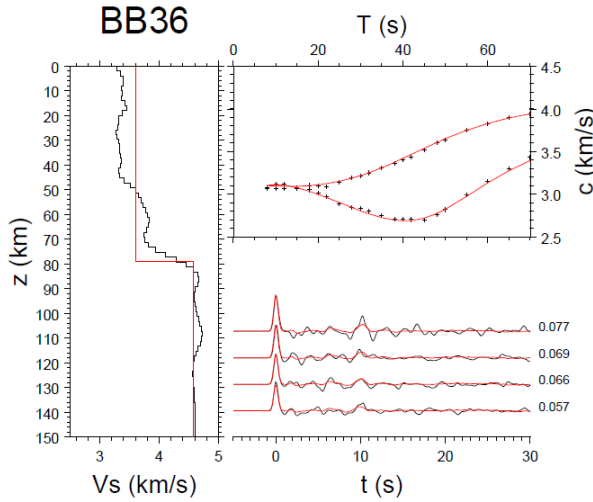


Fig. 1. An example of commonly-used joint inversion of receiver functions and surface wave dispersion. *The left panel shows the S velocity model (black lines) from the inversion and the H-k stacking result (red lines). The right panel shows receiver function and surface wave dispersion fits, black represents data and red represents prediction from the obtained S velocity model. The V_p/V_s ratios are fixed using the values obtained from the H-k stacking results.*

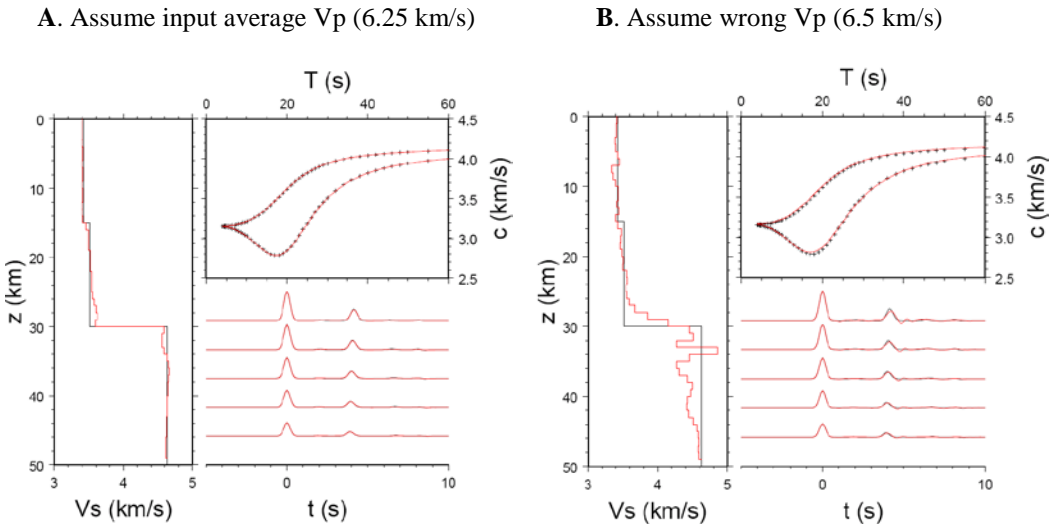


Fig. 2. Synthetic tests on combining Pn station delays with receiver functions and surface wave dispersion for a joint inversion. *The input model is listed in Table 1. (A) Correct average crustal V_p (6.25 km/s) is assumed, which would yield the correct Moho depth (30 km) from Pn station delays. (B) Average crust V_p is assumed to be a wrong value of 6.5 km/s, yielding Moho depth of 33.3 km from Pn station delays. The S structure recovered in B is considerably poorer than in A and has a Moho (slightly less than 30 km) inconsistent with the Pn Moho (33.3 km).*

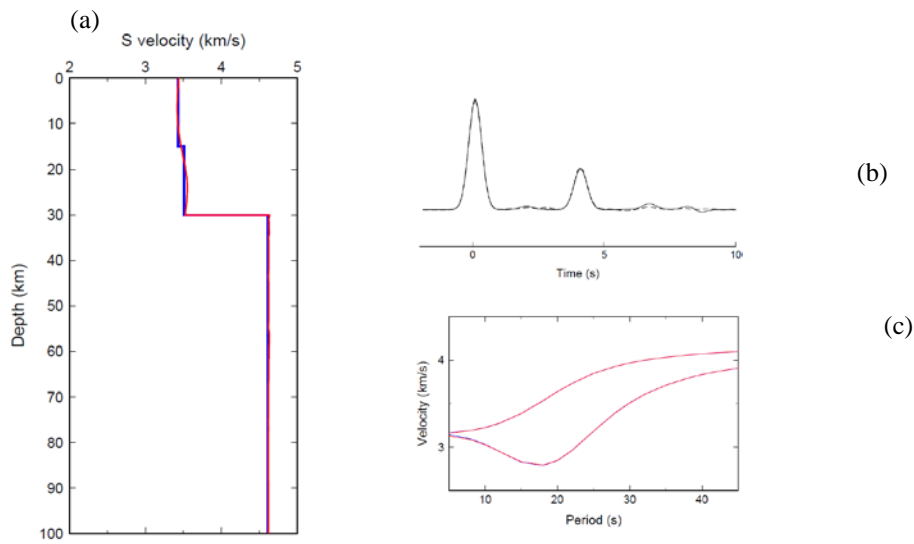


Fig. 3. Synthetic test of joint inversion including receiver functions, surface wave dispersion and Pn delay time data using the Neighborhood Algorithm. *The input velocity model is shown in blue in (a). The input model consists of three layers. The Moho discontinuity is at 30 km depth. The V_p/V_s ratios in the crustal layers are 1.75 and 1.85, respectively. Two sets of splines are used in the inversion. Each set consists of 5 evenly spaced nodes. The output velocity model is plotted in red in (a). Note the velocity jump in the crust is smoother than in the input model due to the natural smoothness of the spline function. An average V_p/V_s ratio of 1.80 in the crust is obtained during searches when Pn delay time data are included. The input (solid line) and output (dashed line) of receiver function waveforms are shown in (b). Only the first 10 seconds of the receiver functions are used in the inversion. Rayleigh wave group and phase dispersion data (blue) from 5 s to 45 s are used in the inversion (c). The corresponding dispersion predictions from the output model are shown in red.*

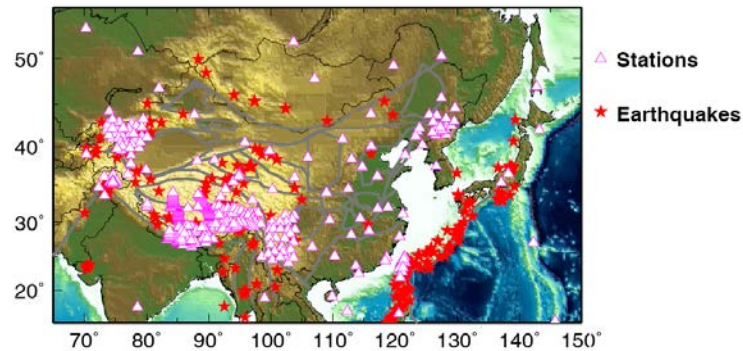


Fig. 4. Distributions of seismic stations (triangles) and earthquakes (stars) used for joint ambient noise and earthquake surface wave tomography.

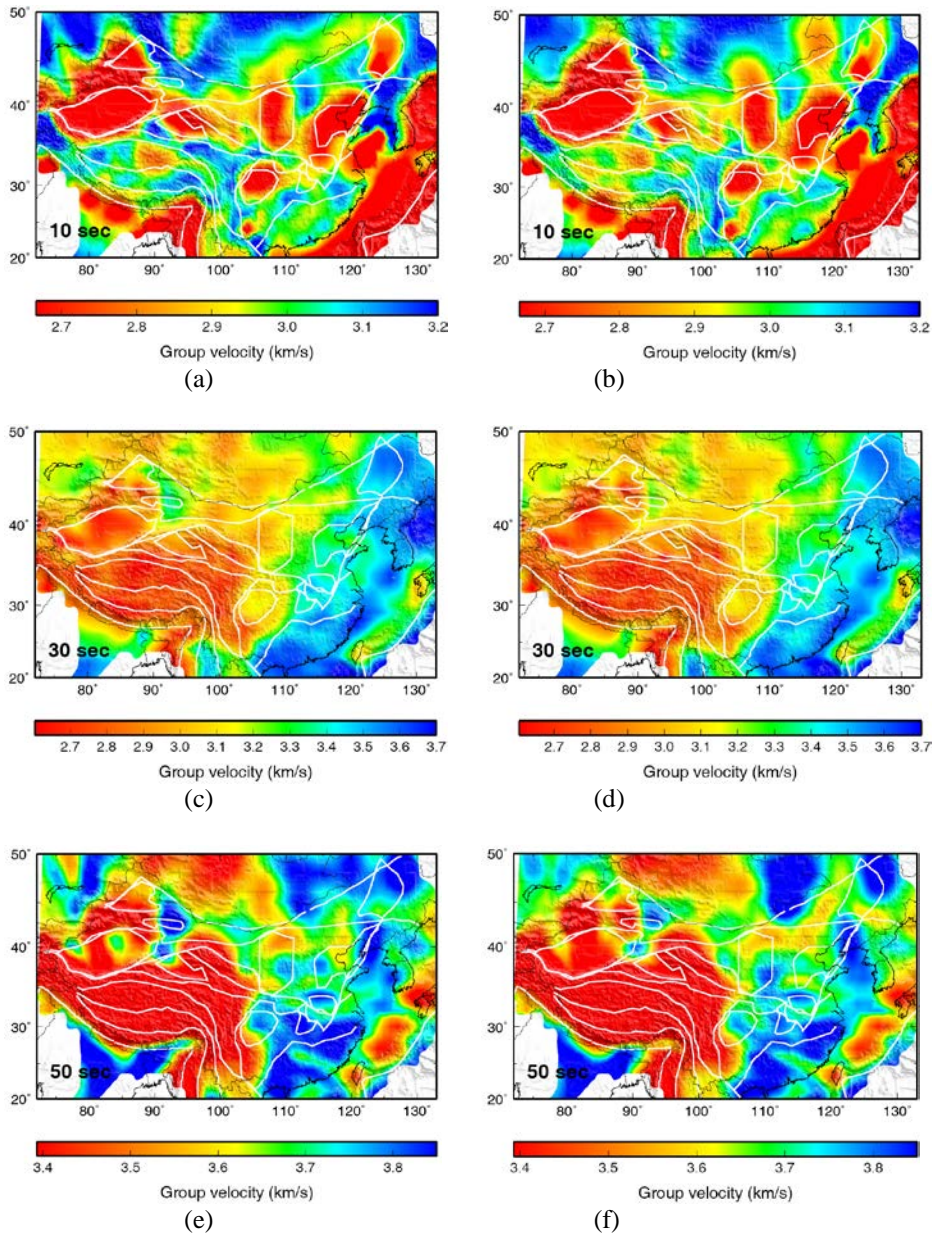


Fig. 5. Group velocity maps at 10, 30, and 50 s using EGFs and earthquake data (left) and earthquake data only (right). Results from two different data sets are generally consistent.

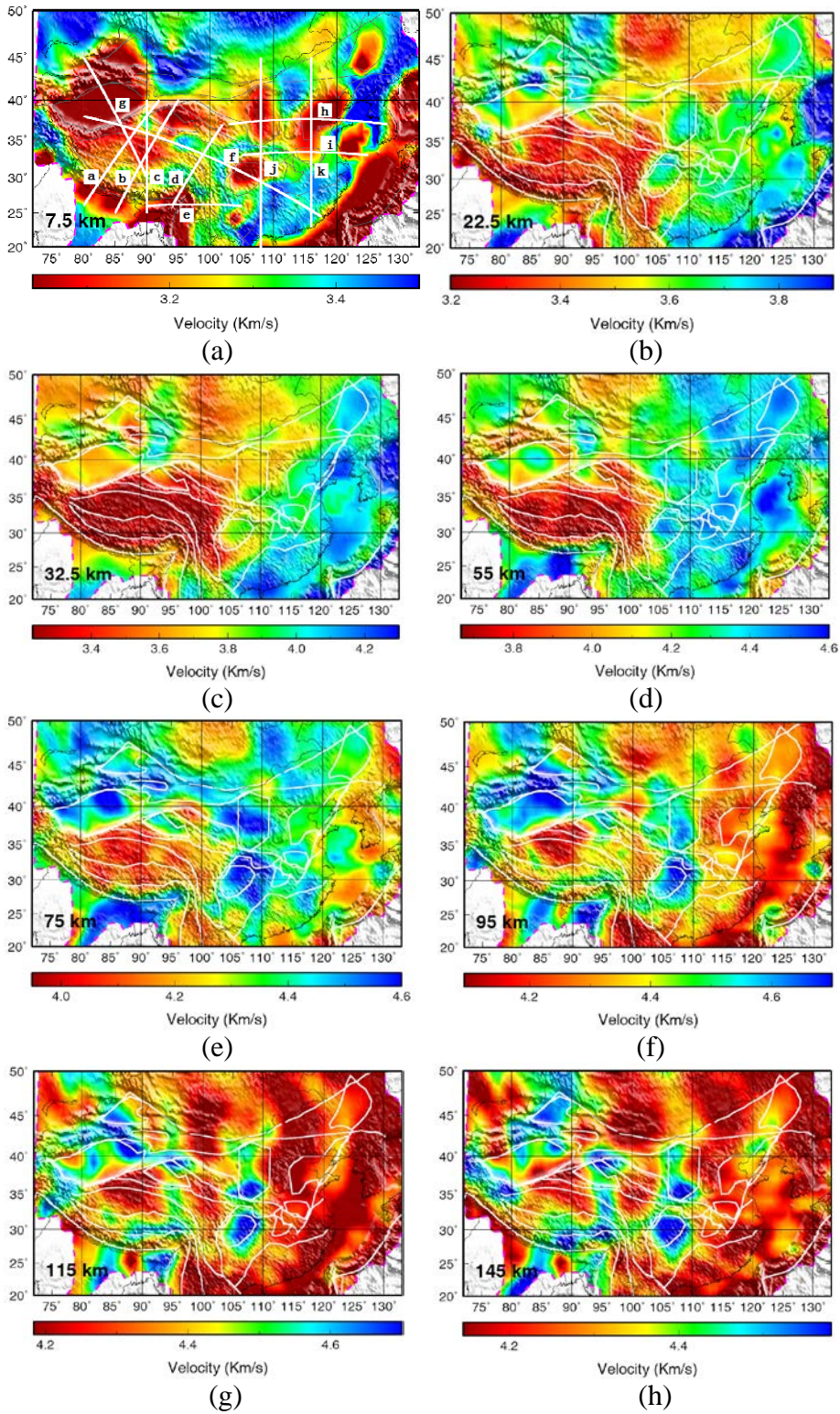


Fig. 6. S velocity maps at different depths from our inverted model. White great circle paths in (a) indicate the cross sections shown in Fig. 7.

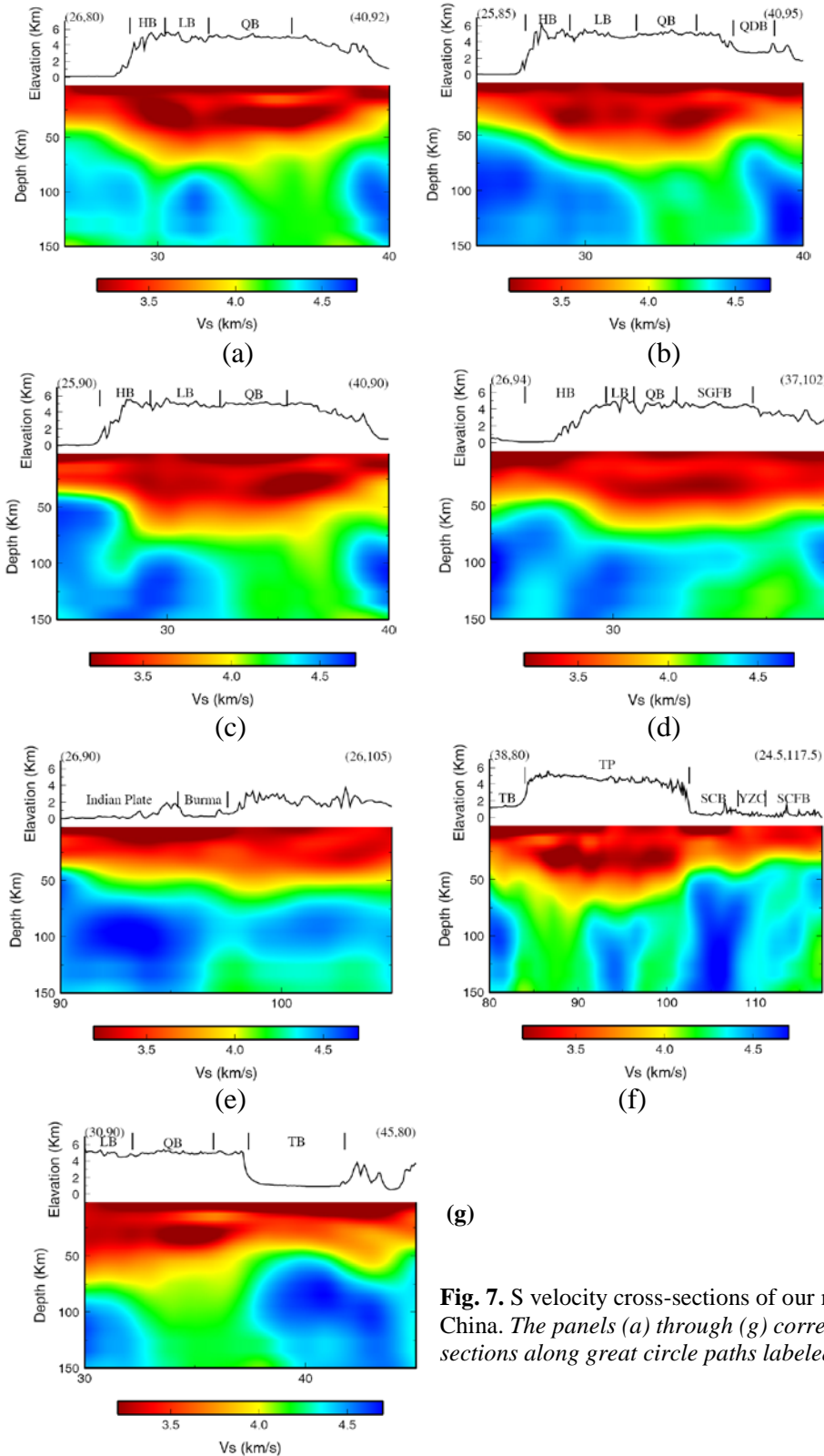


Fig. 7. S velocity cross-sections of our model in western China. The panels (a) through (g) correspond to the cross sections along great circle paths labeled in Fig. 6a.

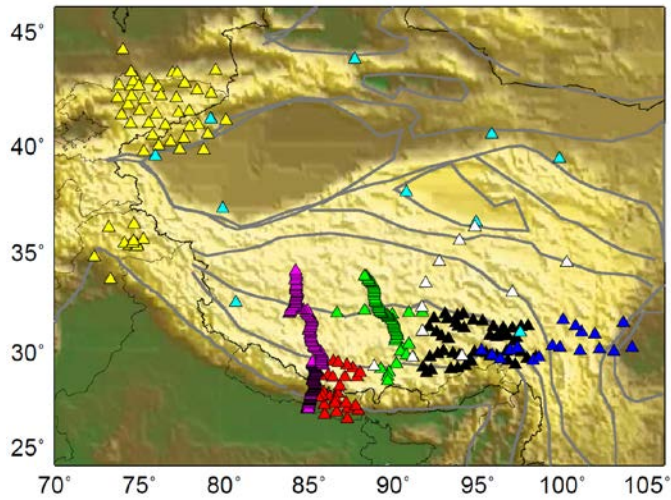


Fig. 8. Stations for which receiver functions have been systematically processed and obtained for the joint inversion of this project.

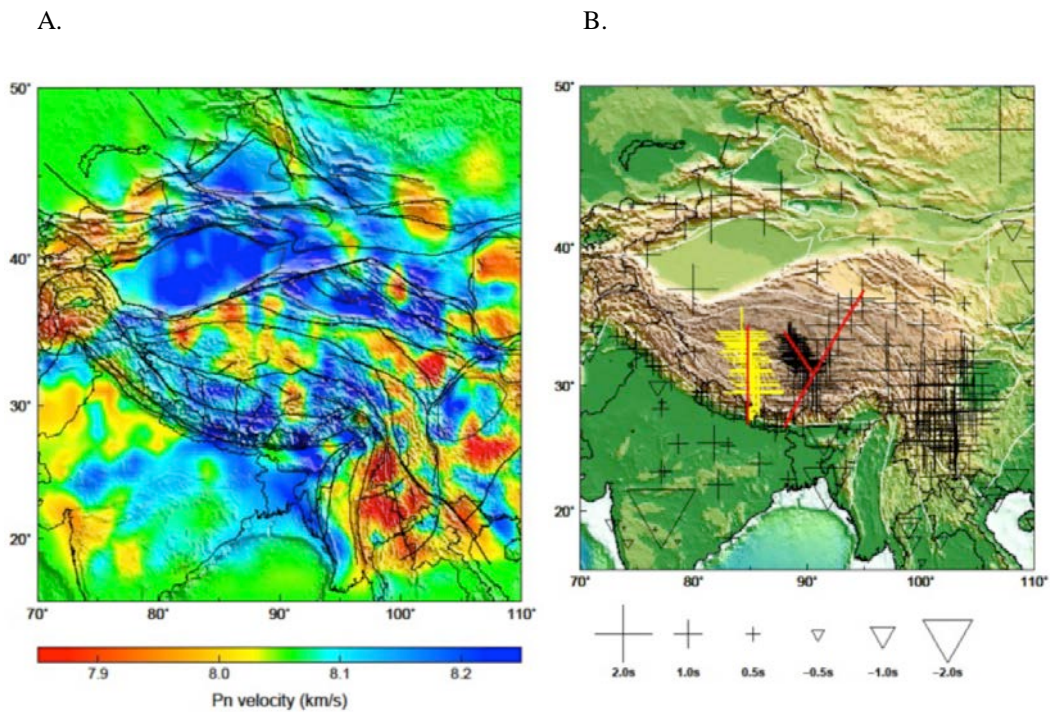


Fig. 9. Results of preliminary Pn tomography in western China. (A) Pn velocity map. (B) Station delays. The number of stations is around 400, including bulletin stations and PASSCAL stations.

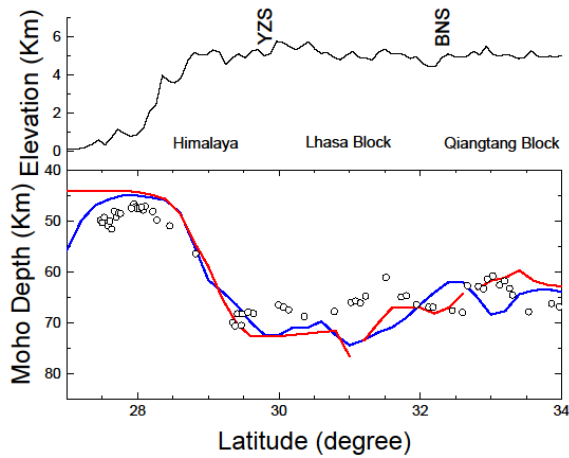


Fig. 10. Crustal thickness along the profile of HI-CLIMB stations. Circles are Moho depths calculated from the Pn station delays for each station. The red line is the approximated Moho location from the receiver function study by Nabelek et al., (2009) using HI-CLIMB stations. The blue line is the approximated Moho location from joint inversion of receiver function and surface wave dispersion by Xu et al. (2013). The topography of Tibetan Plateau is shown on the top of the figure.

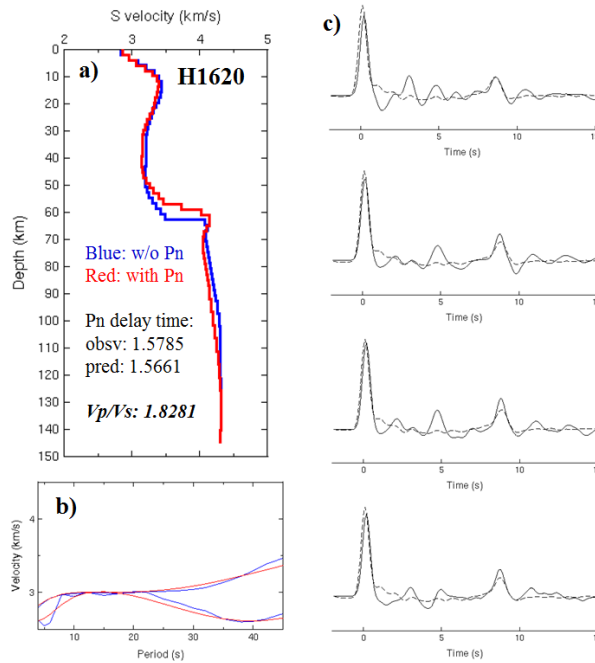


Fig. 11. Test result of joint inversion with Pn data on HiClimb station H1620. a) S velocity profile result with Pn data (red line with the obtained V_p/V_s and the fit to Pn delay time labeled), compared with the result without Pn (blue line); b) The fit for surface wave dispersion curves (observation in blue and prediction in red), including group velocity (lower values) and phase velocity (higher values); c) The fit for 4 receiver functions with different ray parameters (receiver function data are in solid lines and predicted waveforms are in dashed lines).

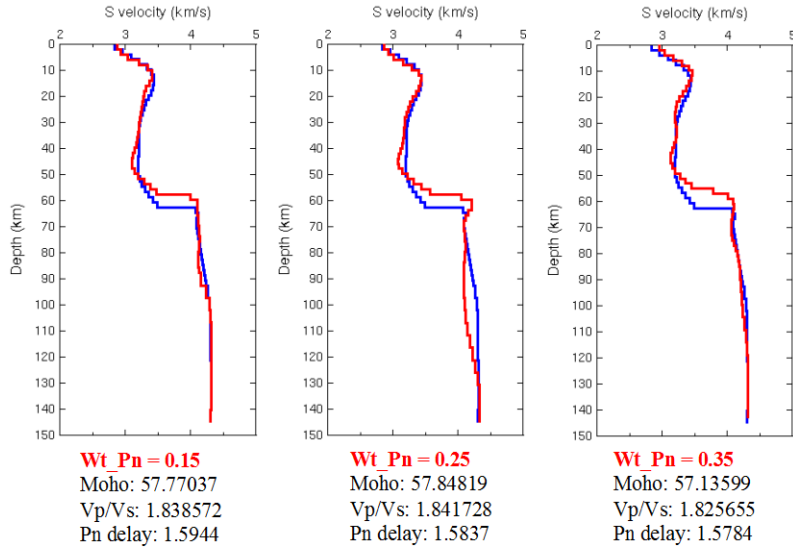


Fig. 12. Tests of Pn weighting on the inversion results (using HiClimb station H1620). The blue curve is the result from inversion of dispersion and receiver functions. The red curves are joint inversions with the addition of Pn data with different Pn weightings as labeled.

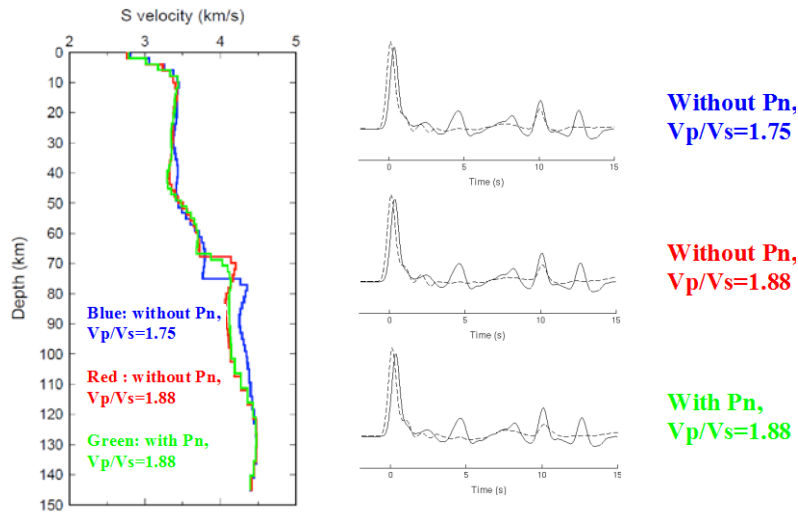


Fig. 13. Tests of model sensitivities to Vp/Vs ratio and with/without Pn data constraint. The example is for HiClimb station H1350. The initial Vp/Vs value is set to 1.75. The optimal value of Vp/Vs from surface wave dispersion, receiver functions, and Pn station delays is found to be 1.88.

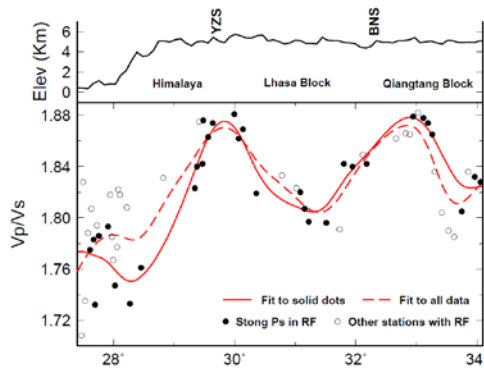


Fig. 14. V_p/V_s ratios derived from joint inversion of surface wave dispersion, receiver functions, and Pn station delays. The stations are from the HiClimb array. The curves are spline fits to the data. Solid dots show the results from the stations with the “best” Moho conversions (a total of 32 stations). Open circles show the results for all the stations that have all three types of data (a total of 60 stations).

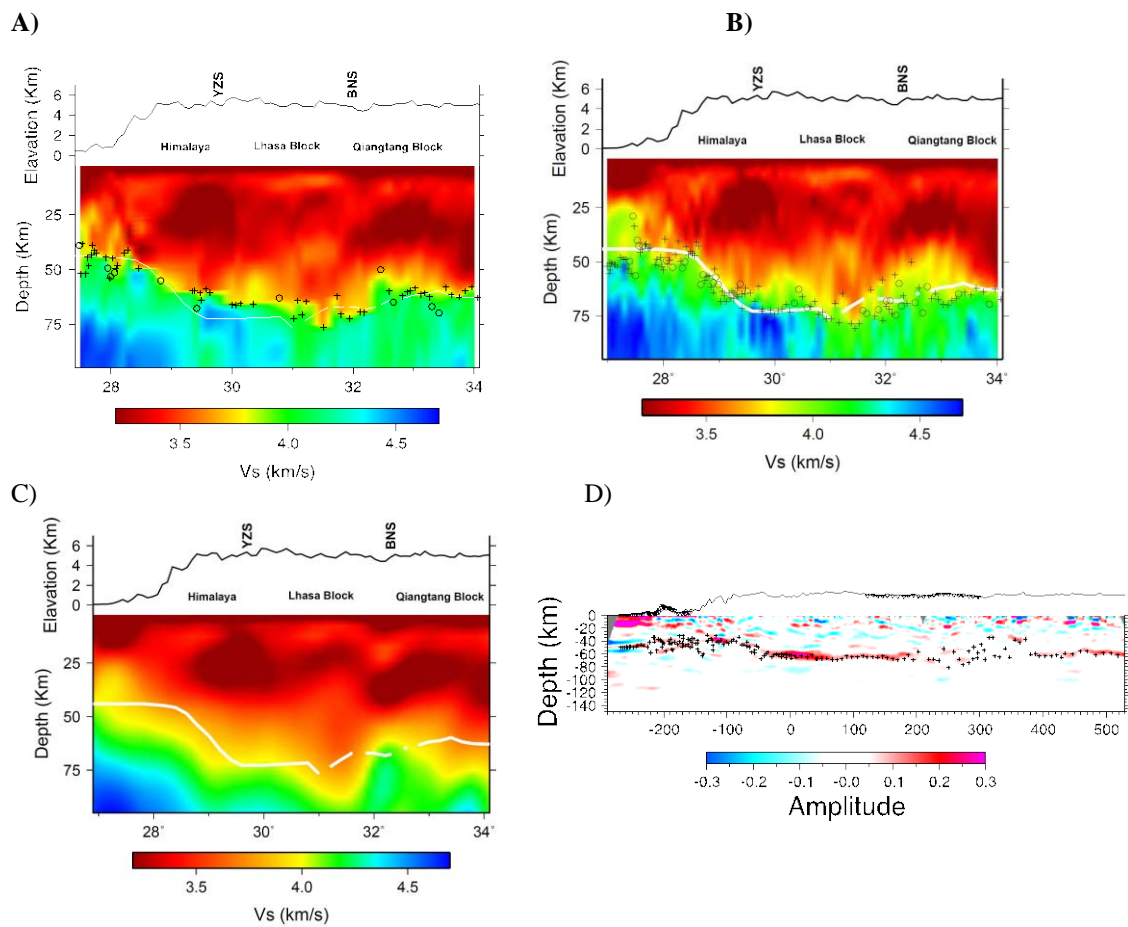


Fig. 15. Results of joint inversion for the Hi-CLIMB array (A, B). Crosses and circles indicate the Moho depth under the stations. Crosses indicate a strong Moho discontinuity while circles mark a gradual Moho velocity transition. (A) shows the joint inversion with the three types of data and (B) shows the joint inversion with dispersion and receiver functions only. Shown in comparison are results from surface wave dispersions only (C) and from common conversion point stacking of the receiver functions only (D). The thick white line is the approximated Moho location from the receiver function study by Nabelek et al. (2009) using the same Hi-CLIMB stations.

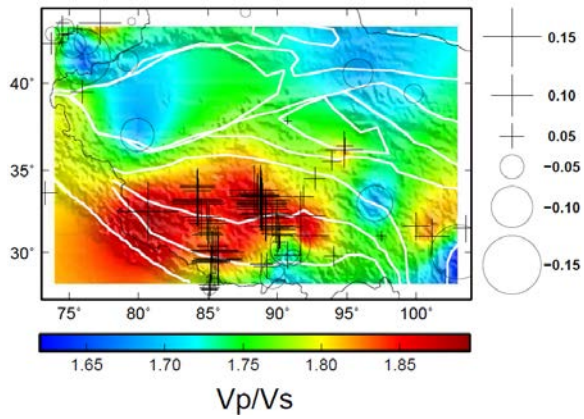


Fig. 16. Map of V_p/V_s ratios in western China obtained in this study. *The symbols are from joint inversions and colors are from interpolation.*

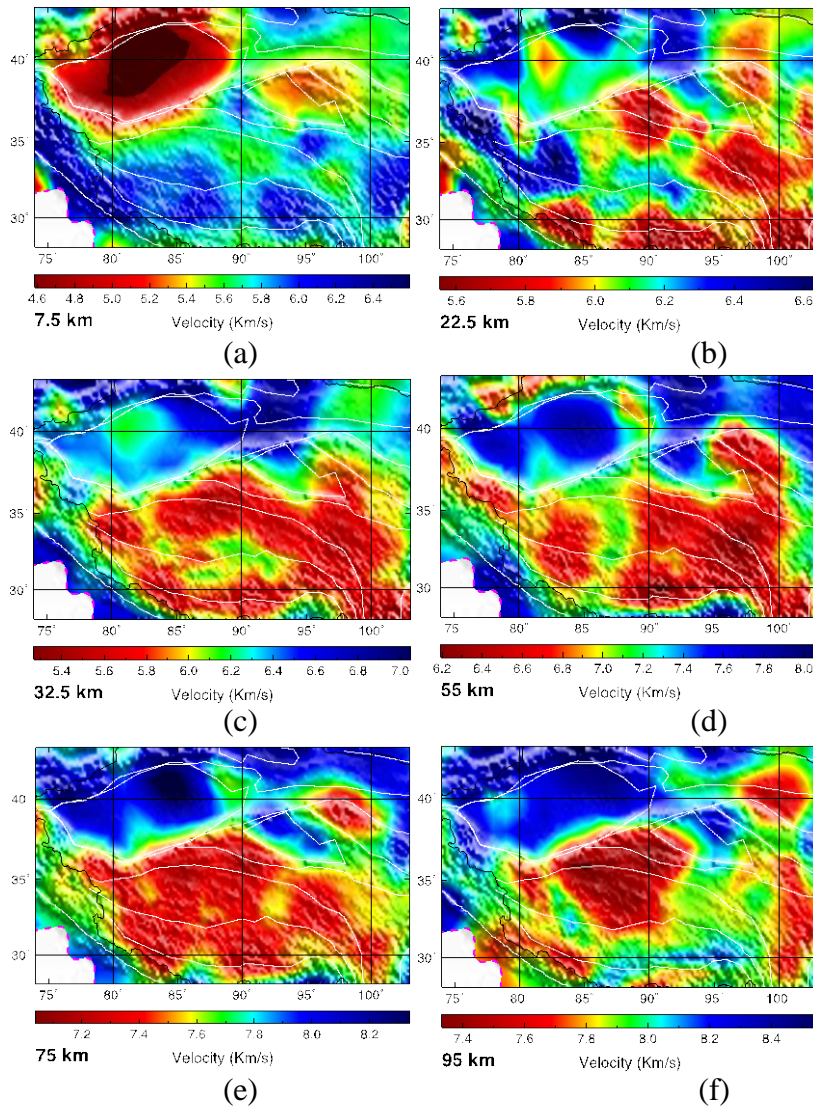


Fig. 17. Maps of the P velocity model of western China from this project.

References

- Ammon, C. J., G. E. Randall, and G. Zandt, On the non-uniqueness of receiver function inversions, *J. Geophys. Res.*, 95(B10), pp. 15303-15318, 1990.
- Benson, G., et al., Processing seismic ambient noise data to obtain reliable broad-band surface wave dispersion measurements, *Geophys. J. Int.*, 169(3), pp. 1239-1260, 2007.
- Hearn, T. M., Anisotropic Pn tomography in the western United States, *J. Geophys. Res.*, 101, pp. 8403-8414, 1996.
- Herrmann, R. B., *Computer Programs in Seismology, Version 3.30*, St. Louis University: Department of Earth and Atmosphere Sciences, 1991.
- Julia, J., C. J. Ammon, R. B. Herrmann, and A. M. Correig, Joint inversion of receiver functions and surface-wave dispersion observations, *Geophys. J. Int.*, **143**, pp. 99-112, 2000.
- Lees, J. M. and R. S. Crosson, Tomographic inversion for three-dimensional velocity structure at Mount St. Helens using earthquake data, *J. Geophys. Res.*, 94, pp. 5716-5728, 1989.
- Liang, C., X. Song, and J. Huang, Tomographic inversion of Pn travel times in China, *J. Geophys. Res.*, 109, B11304, doi:10.1029/2003JB002789, 2004.
- Liang, C. T. and X. D. Song, A low velocity belt beneath northern and eastern Tibetan Plateau from Pn tomography, *Geophys. Res. Lett.*, 33, L22306, 2006.
- Nabelek, J., et al., Underplating in the Himalaya-Tibet collision zone revealed by the Hi-CLIMB experiment, *Science*, **325**, pp. 1371-1374, 2009.
- Nafe, J. E. and C. L. Drake, Physical properties of marine sediments, In Hill, M. N. (Ed.) *The Sea (Vol. 3)*: New York (Interscience), pp. 794-815, 1963.
- Ozalaybey, S., M. K. Savage, A. F. Sheehan, J. N. Louie, and J. N. Brune, Shear-wave velocity structure in the northern basin and range province from the combined analysis of receiver functions and surface waves, *Bull. seism. Soc. Am.*, 87, pp. 183-189, 1997.
- Sambridge, M., Geophysical inversion with a Neighborhood Algorithm –I, Searching a parameter space, *Geophys. J. Int.*, **138**, pp. 479-494, 1999.
- Xu, Z. J., X. D. Song, and L. P. Zhu, Crustal and uppermost mantle S velocity structure under Hi-CLIMB seismic array in central Tibetan Plateau from joint inversion of surface wave dispersion and receiver function data, *Tectonophysics*, 584, pp. 209-220, doi:10.1016/j.tecto.2012.08.024, 2013a.
- Xu, Z. J., X. D. Song, and S. H. Zheng, Shear velocity structure of crust and uppermost mantle in China from surface wave tomography using ambient noise and earthquake data, *Earthq. Sci.*, in press, 2013b.
- Zhu L. P. and H. Kanamori, Moho depth variation in southern California from teleseismic receiver functions, *J. Geophys. Res.*, 105(B2), pp. 2969-2980, 2000.

DISTRIBUTION LIST

DTIC/OCP 8725 John J. Kingman Rd, Suite 0944 Ft Belvoir, VA 22060-6218	1 cy
AFRL/RVIL Kirtland AFB, NM 87117-5776	2 cys
Official Record Copy AFRL/RVBYE/Robert Raistrick	1 cy

This page is intentionally left blank.